How to reconstruct aerosol-induced diffuse radiation scenario for simulating GPP in land surface models? An evaluation of reconstruction methods with ORCHIDEE_DFv1.0_DFforc

Yuan Zhang[1,2], Olivier Boucher[3], Philippe Ciais[1], Laurent Li[2], and Nicolas Bellouin[4]

[1]Laboratoire des Sciences du Climat et de l'Environnement (LSCE), IPSL, CEA/CNRS/UVSQ, Gif sur Yvette, France
[2]Laboratoire de Météorologie Dynamique, IPSL, Sorbonne Université/CNRS, Paris, France
[3]Institut Pierre–Simon Laplace, CNRS/Sorbonne Université, Paris, France
[4]Department of Meteorology, University of Reading, Reading, RG6 6BB, UK

Correspondence: Yuan Zhang (yuan.zhang@lmd.jussieu.fr)

Abstract. The impact of diffuse radiation on photosynthesis has been widely documented in field measurements. This impact may have evolved over time during the last century due to changes in cloudiness, increased anthropogenic aerosol loads over polluted regions, and to sporadic volcanic eruptions curtaining the stratosphere with sulfate aerosols. The effect of those changes in diffuse light on large-scale photosynthesis (GPP) are difficult to quantify, and land surface models have been designed to simulate them. Investigating how anthropogenic aerosols have impacted GPP through diffuse light in those models requires carefully designed factorial simulations and a reconstruction of background diffuse light levels during the pre-industrial period. Currently, it remains poorly understood how diffuse radiation reconstruction methods can affect GPP estimation and what fraction of GPP changes can be attributed to aerosols. In this study, we investigate different methods to reconstruct spatio-temporal distribution of the fraction of diffuse radiation (Fdf) under pre-industrial aerosol emission conditions using a land surface model with a two-stream canopy light transmission scheme that resolves diffuse light effects on photosynthesis in a multi-layered canopy, ORCHIDEE_DF. We show that using a climatologically-averaged monthly Fdf, as has been done by earlier studies, can bias the global GPP by up to 13 PgC yr^{-1} because this reconstruction method dampens the variability of Fdf and produces Fdf that is inconsistent with short-wave incoming surface radiation. In order to correctly simulate pre-industrial GPP modulated by diffuse light, we thus recommend that the Fdf forcing field should be calculated consistently with synoptic, monthly and inter-annual aerosol and cloud variability for pre-industrial years. In the absence of aerosol and cloud data, alternative reconstructions need to retain the full variability in Fdf. Our results highlight the importance of keeping consistent Fdf and radiation for land surface models in future experimental designs that seek to investigate the impacts of diffuse radiation on GPP and other carbon fluxes.

Copyright statement. TEXT

1 Introduction

Gross primary production (GPP) is one of the largest carbon fluxes in the global carbon cycle and the only way by which land ecosystems capture CO_2 from the atmosphere. The GPP of terrestrial ecosystems is known to be sensitive to climate factors including temperature, precipitation and incoming shortwave radiation (Nemani *et al.* , 2003). During the recent two decades, several *in situ* studies reported that in addition to the total amount of incoming shortwave radiation, the fraction of diffuse radiation (Fdf) as a part of the total radiation can also strongly affect GPP and in turn the carbon cycle (Gu *et al.* , 2002, 2003; Niyogi *et al.* , 2004). For a given level of incoming radiation, conditions with more diffuse light are found to increase light use efficiency by 6-180% in different vegetation types (Alton *et al.* , 2007; Choudhury, 2001; Gu *et al.* , 2002), which will increase the total GPP. This is because that the diffuse radiation can penetrate deeper and reach more shaded leaves in the deep canopy and consequently enhance the canopy photosynthesis. In other words vegetation is sensitive to both light quantity and quality.

This effect of diffuse radiation is potentially an important explanation of observed large-scale trends of GPP because the aerosol emissions from anthropogenic activities have increased, and the light-scattering properties of those aerosols augment the diffuse fraction of light. In addition, sporadic volcanic eruptions inject aerosols in the stratosphere which decrease the amount of light reaching the surface and strongly increase its diffuse fraction globally during a few years after each eruption. However, the large scale impacts of aerosol-induced light quality changes remain poorly quantified. The recent development of land surface models (LSMs) that distinguish direct and diffuse light in canopy light transmission (Dai *et al.* , 2004; Alton *et al.* , 2007; Mercado *et al.* , 2009; Chen , 2013; Yue and Unger , 2017; Zhang *et al.* , 2020) provides an opportunity to study how diffuse light and other climate variables affect GPP and its variability.

In spite of the increasing number of LSMs considering diffuse light, there remains no standard experimental design for isolating the impacts of aerosol-induced diffuse radiation changes on GPP. Alton *et al.* (2007) compared equivalent simulations performed with two LSMs, one with a one-stream and the other one with a two-stream canopy light transmission scheme accounting for diffuse and direct light effects on GPP. In contrast, Mercado *et al.* (2009) designed, two scenarios with and without changes in Fdf, using the same LSM, keeping all other climate forcing variables identical. Rap *et al.* (2018) and Yue and Unger (2018) also used simulations under different scenarios, but with different reconstructions of Fdf. Currently, the lack of harmonized design for modeling GPP from diffuse light still prevents the comparison of those different results to understand the magnitude and uncertainties of aerosol impacts. Therefore, a rigorous simulation design for LSMs resolving diffuse light effects is urgently needed.

Because the one-stream and two-stream canopy light transmission models do not necessarily give the same GPP when there is no changes in Fdf, it is difficult to interpret the GPP difference detected by the two LSMs in Alton *et al.* (2007) as impacts of diffuse radiation changes. In contrast, considering factorial simulations with the same LSM capable of resolving diffuse light effects, underwith different diffuse light forcing scenarios, e.g., the scenario with actual anthropogenic aerosol emissions and the one with aerosol emissions at pre-industrial level (before or in early 20th century), removes the interference from different model structures. However, attention has to be paid on how to define the forcing of pre-industrial aerosols in the baseline simulation. Currently, there are mainly two possible approaches to reconstruct pre-industrial diffuse light forcing,

given gridded fields of all other climate variables needed as input for a given LSM. The first approach relies on the climate and diffuse light fields from Earth system models (ESMs) runs with and without anthropogenic aerosol emission scenarios. This approach can provide a full set of climate variables without anthropogenic aerosols, which defines the baseline, but suffers from large climate biases and uncertainties from ESMs, which inevitably leads to large biases in the modeled GPP (Zhang *et al.* , 2019). Furthermore, ensemble simulations with ESMs may also be required to detect and attribute the impacts of anthropogenic aerosols from natural climate variability, which unavoidably arises when different simulations are performed. Such a detection/attribution framework (Eyring *et al.* , 2016) is used for attributing the effect of human induced radiative forcing on climate change, but requires large ensemble of ESM simulations, often at the cost of reduced spatial resolution. The other approach relies on using reconstructed gridded climate fields based on observations and adding to these fields the variability of the Fdf. Compared to using ESM climate, the reconstructed climate is more accurate. However, a counterfactual reconstruction with constant pre-industrial aerosols during the entire historical period is not available. To investigate the anthropogenic aerosol impacts, such a "pre-industrial or no-anthropogenic aerosol scenario" must thus be reconstructed based on careful assumptions.

For the sake of isolating the impacts of aerosol-induced light quality changes, the problem is thus to reconstruct a no-anthropogenic-aerosol multi-year baseline pre-industrial forcing that keeps the Fdf at the pre-industrial level but retains the natural variation of shortwave light and of all other climate fields. Mercado *et al.* (2009) opted to prescribe a monthly mean climatology of Fdf in their pre-industrial baseline scenario. This is a coarse approximation because Fdf has a strong covariance with all other climate variables, especially shortwave radiation. For instance, a sunny month of January in a given year cannot have the same mean Fdf value as a very cloudy January in another year. Similarly, a sunny 1st of July in one grid-cell cannot be assigned the same Fdf as a cloudy 1st of July happening another year. The averaging used by Mercado *et al.* (2009) inevitably causes a mismatch between Fdf and other climate forcing variables. Considering the non-linear response of GPP to Fdf for different climate forcing conditions, the monthly mean climatology approach to reconstruct pre-industrial Fdf may cause biases in the baseline GPP and consequently on the attribution of the historical anthropogenic aerosol impacts on GPP changes examined against this baseline. In this study, we study a set of simulations using different diffuse light reconstructions to evaluate the impacts of the reconstruction method on the simulated anthropogenic-aerosol impacts on GPP during the historical period (1901–2012) using the recently developed ORCHIDEE-DF LSM which has a two-stream canopy light transmission scheme and accounts for Fdf and climate effects on GPP over the whole globe. The main objectives of this study are the following: i) investigate whether and by how much the Fdf baseline pre-industrial reconstruction method affects GPP; ii) identify the underlying mechanisms of the modeled GPP dependence upon the chosen reconstruction method; and iii) recommend a best reconstruction method for future studies, that could be adopted by other LSMs resolving diffuse light impacts.

2   Data and Methods

2.1   Model Description

In order to simulate the impact of diffuse radiation, we used the ORCHIDEE_DF LSM, which is originally based on the ORCHIDEE LSM trunk (v5453) (Krinner *et al.* , 2005), but has a two-stream canopy radiation transmission module to dis-

tinguish direct and diffuse radiation (Zhang *et al.* , 2020). ORCHIDE_DF has been evaluated using obervations from 159 flux sites over the globe and was proven to be able to reproduce the observed GPP sensitivity to diffuse light (Zhang *et al.* , 2020) under the same light and other climate fields conditions. Instead of using the empirical light partitioning module of

90   the original ORCHIDEE_DF that calculated Fdf from shortwave radiation and solar angle (Zhang *et al.* , 2020), we modified the model to let it read Fdf from gridded forcing files, along with other climate variables. Due to the new canopy light transmission scheme, the model need to be recalibrated to obtain C fluxes that match observation-based estimations. Here, we empirically tuned the photosynthesis-related parameters (Vcmax, specific leaf area, leaf age) within some reasonable ranges to simulate similar GPP as in the TRENDY V8 S3 simulation performed with the ORCHIDEE trunk version for each plant func-

95   tional type and during the 1900s. We chose the TRENDY V8 S3 simulation as the reference because the ORCHIDEE trunk version for this simulation has been well-tuned to simulate C fluxes matching the observation-based global carbon budget (http://sites.exeter.ac.uk/trendy/), also due to the easy accessibility of data.

2.2   Forcing data and experimental design

The climate forcing used in this study is the 6-hour CRUJRA v1.1 dataset (Harris *et al.* , 2014; Harris, 2019; Kobayashi, 2015).

100   CRUJRA v1.1 dataset was generated by adjusting the Japanese Reanalysis data (JRA) produced by the Japanese Meteorological Agency (JMA) with the observationally-based monthly Climatic Research Unit (CRU) TS 3.26 data. It provides 6-hourly meteorological variables at $0.5 \times 0.5°$ resolution including 2-metre air temperature, total precipitation, downward shortwave radiation, downward longwave radiation, 2-meter specific humidity, air pressure and the zonal and meridional components of the 10-m wind. This dataset is the standard forcing input used in the TRENDY v7 simulations (http://sites.exeter.ac.uk/trendy/).

105   For the sake of investigating the effect of diffuse radiation with a framework consistent with the TRENDY simulation protocol (http://sites.exeter.ac.uk/trendy/), a new Fdf field during 1900-2017 was calculated along with the above-mentioned climate variables at the same spatial and temporal resolutions. The radiative transfer calculations to obtain the Fdf field are based on monthly-averaged tropospheric and stratospheric aerosol optical depth, and 6-hourly cloud fraction. The tropospheric aerosol optical depth of each aerosol type is from the HadGEM2-ES historical and RCP8.5 simulations (Bellouin *et al.* , 2011).

110   To correct the biases in HadGEM2-ES, tropospheric aerosol optical depths are scaled over the entire period to match the global and monthly averages obtained by the CAMS Reanalysis of atmospheric composition for the period 2003-2017 (Inness *et al.* , 2019), which assimilates satellite retrievals of aerosol optical depth. The stratospheric aerosol optical depth is from the climatology by Sato *et al.* (1993), which has been updated to 2012. Years after 2012 are assumed to be background years without significant influence of volcanoes and the stratospheric aerosol optical depth is assumed to be the same as a recent

115   background year 2010. This assumption is supported by the Global Space-based Stratospheric Aerosol Climatology time series (1979-2016; (Thomason *et al.* , 2018)). The time series of cloud fraction is derived from the 6-hourly cloud distributions simulated by the Japanese Reanalysis (JRA; (Kobayashi, 2015)) and is scaled to match the monthly-averaged cloud cover in the CRU TS v4.03 dataset (Harris *et al.* , 2014). The surface radiative fluxes calculation considered aerosol-radiation interactions from both tropospheric and stratospheric aerosols, and for aerosol-cloud interactions from tropospheric aerosols, except mineral

120   dust. The radiative effects of aerosol-cloud interactions are assumed to scale with the radiative effects of aerosol-radiation

interactions, and regional scaling factors derived from HadGEM2-ES are used in the calculation. Atmospheric constituent other than aerosols and clouds are set to a constant standard mid-latitude summer atmosphere, but their variations do not affect the diffuse fraction of surface shortwave fluxes.

To evaluate the methods reconstructing baseline Fdf under pre-industrial aerosol conditions, we first selected only the volcano-free years during 1901-1920 (Table 1) when there were negligible volcanic aerosol emissions and anthropogenic aerosol emissions were about a third of their present-day rates to affect Fdf. Based on the assumption that this sample is representitive to the pre-industrial aerosol conditions, four methods are used to reconstruct 0.5° x 0.5° 6-hourly pre-industrial Fdf field and corresponding simulations are set up during 1901-2017. The first method, noted as *DF-PI-MON-CLIM* , is based on a monthly climatology mean, i.e. all the 6-hour time steps within a certain month take the same value from the mean Fdf of this month across the selected years. This method is similar to the approach used by Mercado *et al.* (2009). The second method accounts for the fact that there is a strong diurnal cycle of Fdf. This diurnal cycle is important because the diffuse light impact on GPP is not the same at different time of a day due to different radiation levels. In order to retain the diurnal cycle of Fdf, the second method, named *DF-PI-6H-CLIM* , uses a 6-hour climatological mean across the selected years:

$$Fdf_f(t) = \frac{\sum_y Fdf_o(y,t)}{\sum_y y} \tag{1}$$

where $Fdf_f(t)$ is the final Fdf at time step t, $Fdf_o(y,t)$ is the original Fdf at time step t of year y. This method accounts for the periodical diurnal decrease of Fdf from morning to mid-day and its increase from mid-day to afternoon, but it ignores the variability of Fdf between years. For instance, the same time step may be very sunny with low Fdf in one year but completely cloudy with high Fdf in other. The *DF-PI-6H-CLIM* reconstruction smooths the Fdf and give medium Fdf for both years, which is not realistic (Fig. 1). The third method avoids this smoothing of the variability of Fdf and uses Fdf directly from years select from 1901-1920 to have similar average annual Fdf as the previous two reconstructions. Because the Fdf variation differs among years, to understand the uncertainty caused by this difference, we use an ensemble of three members, *DF-PI-1901*, *DF-PI-1905* and *DF-PI-1916*, which respectively repeat the Fdf field of 1901, 1905 and 1916 to the entire simulation period. The final estimation of C fluxes are based on the average of the output of the three members. This reconstruction based on ensemble simulations is named *DF-PI-ENS* . Finally, a new Fdf field, *DF-PI-AERO* , is generated using the same atmospheric radiative transfer model previously described but the anthropogenic emissions were kept at the 1901-1920 level and the volcanic aerosols emissions were excluded.

It should be noted that all the simulations in this study use the same SWdown field because the target of this study is to understand the impact from aerosol-induced radiation quality, i.e. Fdf, changes only. In reality, the aerosols and clouds also cause a coincident change in radiation quantity, i.e. SWdown, which is important to consider when investigating the full impacts for aerosols. But it is out of the scope of this study.

Besides the above-mentioned reconstructions, a historical simulation (*DF-HIST*) driven by the original Fdf is set up as the reference to investigate the impacts of diffuse radiation. Except the Fdf field, all these simulations use the same climate and land use maps which vary throughout the simulations. Also, all these simulations start from the same state of a spin-up simulation

Table 1. Experimental design in this study

Name		Climate and land use maps	Incoming diffuse shortwave radiation fraction
spinup[1]		1901-1920 cycling	1901-1920 cycling
DF-HIST		All variables varying	Varying during the study period
DF-PI-6H-CLIM		All variables varying	Repeat the 6 hour average of 1901, 1904-1906, 1909, 1911, 1915-1920, with diurnal and seasonal variations maintained
DF-PI-MON-CLIM		All variables varying	Repeat the monthly average of 1901, 1904-1906, 1909, 1911, 1915-1920 over all years
DF-PI-ENS[2]	*DF-PI-1901*	All variables varying	Repeat the field of 1901
	DF-PI-1905	All variables varying	Repeat the field of 1905
	DF-PI-1916	All variables varying	Repeat the field of 1916
DF-PI-AERO		All variables varying	Calculated using atmospheric light transfer model with 1901-1920 aerosol level (volcanic aerosols excluded)

[1] All the other simulations start from the stage when C pools are equilibrated (340-yr simulation using the spinup-analytic simulation in ORCHIDEE_DF)

[2] The average of *DF-PI-1901*, *DF-PI-1905*, *DF-PI-1916*

who has equilibrated the C pools using 1901-1920 climate and Fdf. A detailed description of each simulation can be found in Table 1.

3 Results

3.1 Impacts of Fdf changes at the global scale

As shown in Fig. 2a, the historical global mean Fdf has three phases during the entire study period. Before 1950, the mean Fdf varies around 0.615-0.62. During 1950-1980, the mean Fdf increases from 0.62 to 0.64 mainly in response to increasing anthropogenic aerosol emissions (Lamarque *et al.* , 2014). After 1980s, the mean Fdf stays around 0.64. In addition to these three phases, notable spikes of Fdf of 0.02-0.04 are found in years with strong volcanic eruptions, the Santa Maria in 1902-1903, El Chichón in 1982, Mount Pinatubo in 1991. Because the no-anthropogenic-aerosol reconstructions (*DF-PI-6H-CLIM*, *DF-PI-ENS*, *DF-PI-MON-CLIM*) use the volcano-free years during 1901-1920, they produce the same or very similar global yearly mean Fdf around 0.615 during the entire study period. For the (*DF-PI-AERO*) reconstruction, the Fdf increased by about 0.005 after the 1950s, which is not comparable to the increase of Fdf in *DF-HIST*. This increase is mainly due to the changes in cloudiness and natural aerosols.

In response to the different interannual variation of Fdf between the *DF-HIST* and no-anthropogenic-aerosol scenarios, the differences between *DF-HIST* and all no-anthropogenic-aerosol GPP (ΔGPP) also show a 3-phase pattern (Fig. 2b), with the highest ΔGPP occurring after 1960s and during large volcanic eruptions. Although the interannual variation of ΔGPP is similar
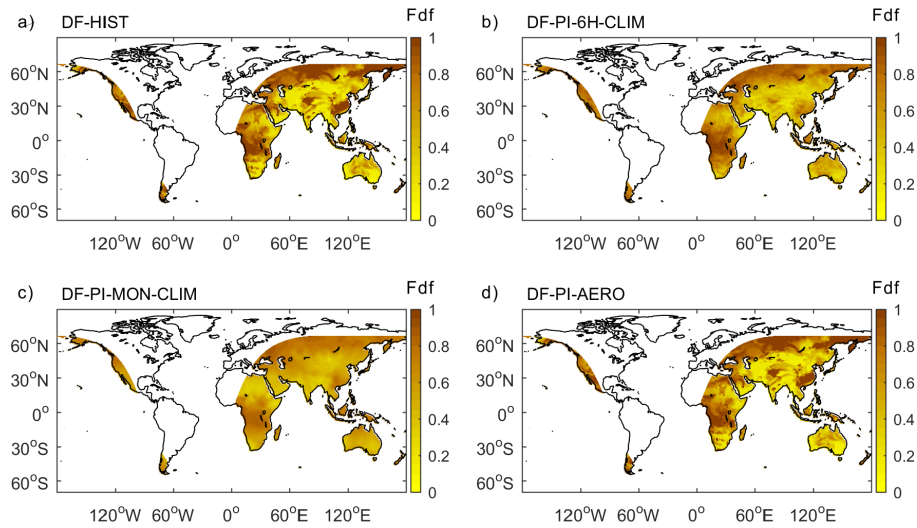
Figure 1. Fdf during 1901-01-01 00:00-06:00 UTC from (a) the original forcing including climate variability from CRU-JRA and historical aerosol concentration (*DF-HIST*), (b) the 6-hour mean of 01-01 00:00-06:00 Fdf over 1901-1920 non-volcanic years (*DF-PI-6H-CLIM*), (c) the monthly mean of January Fdf over 1901-1920 non-volcanic years (*DF-PI-MON-CLIM*), (d) the reconstruction using climate variability from CRU-JRA and mean 1901-1920 aerosol concentration (*DF-PI-AERO*). Night time pixels are masked for comparison.
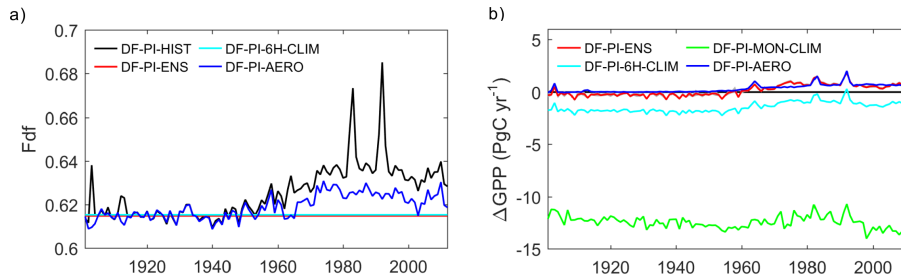
Figure 2. Time series of (a) global mean Fdf and (b) ΔGPP between *DF-HIST* and no-anthropogenic-aerosol scenarios. The *DF-PI-MON-CLIM* has the same mean Fdf as *DF-PI-6H-CLIM*, thus not shown in (a). The shaded area along the red curve in (b) indicates the range of the three ensemble members of the *DF-PI-ENS* simulations.

170 among reconstructions, large discrepancies on the magnitude of global ΔGPP are found. The *DF-PI-ENS* and *DF-PI-AERO* reconstructions show similar global GPP compared with the *DF-HIST* scenario before 1950s. In contrast, the *DF-PI-6H-CLIM* reconstruction leads to a negative ΔGPP of –1.8 PgC yr^{-1} during the same period (1901-1950). The *DF-PI-MON-CLIM* reconstruction results in a much larger negative ΔGPP of over –12 PgC yr^{-1}. Because during 1901-1920, the Fdf of *DF-HIST* and no-anthropogenic-aerosol scenarios are at similar level, the negative ΔGPP from *DF-PI-6H-CLIM* and *DF-PI-MON-CLIM*
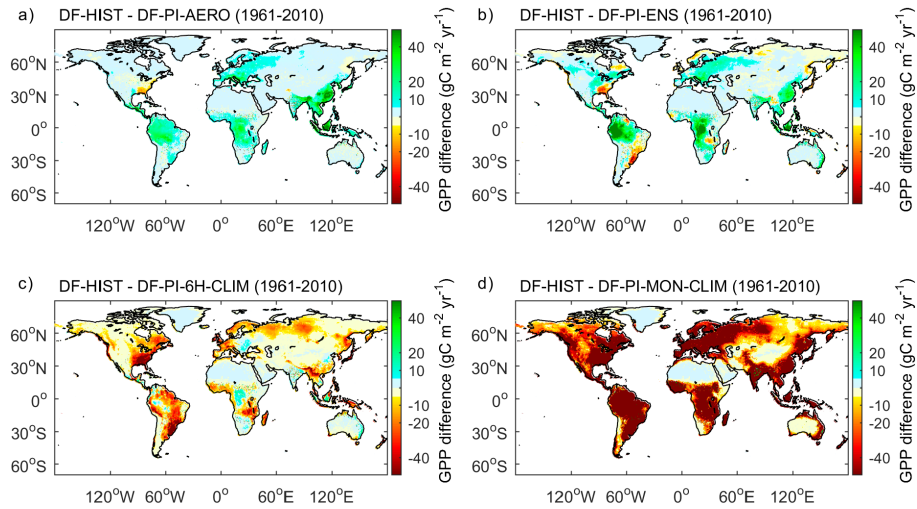175 must be related to the difference from the method chosen for the pre-industrial Fdf reconstruction.

7

Figure 3. Spatial patterns of ΔGPP (in gC m^{-2} yr^{-1}) between *DF-HIST* and (a) *DF-PI-AERO* , (b) *DF-PI-ENS* , (c) *DF-PI-6H-CLIM* and (d) *DF-PI-MON-CLIM* during 1961-2010.

3.2   spatial distribution of ΔGPP

Fig 3 shows the spatial patterns of ΔGPP derived from each reconstruction during the period (1961-2020) when Fdf is most different from the pre-industrial level. Among the four reconstructions, *DF-PI-AERO* and *DF-PI-ENS* reconstructions show positive ΔGPP of over 10 gC m^{-2} yr^{-1} in East and South Asia, Europe and tropical rainforest regions. In spite of this similarity in pattern, *DF-PI-ENS* reconstruction shows higher ΔGPP than PIaero in the West Amazon and Congo basins. Besides, the *DF-PI-ENS* reconstruction has negative ΔGPP in high latitudes and in small patches in eastern Brazil and Uruguay, while the *DF-PI-AERO* shows much smaller regions with negative ΔGPP . In contrast to the positive ΔGPP of *DF-PI-AERO* and *DF-PI-ENS* , the *DF-PI-6H-CLIM* reconstruction shows negative ΔGPP of –10 to –40 gC m^{-2} yr^{-1} in East US, West Europe, South China and large regions of South America. The *DF-PI-MON-CLIM* reconstruction has even larger negative ΔGPP , with magnitude larger than 40 gC m^{-2} yr^{-1}, over almost all vegetated regions.

3.3   Seasonal and diurnal variations of ΔGPP

Because the different Fdf variabilities from different reconstructions can lead to different variations in ΔGPP , we compared the seasonal and diurnal variations of ΔGPP from those different reconstructions at different latitudes (Fig. 4 and 5). At the seasonal scale, the ΔGPP from *DF-PI-AERO* is neutral during 1901-1920 at all seasons while all other reconstructions found negative ΔGPP during this time (Fig. 4). During 1993-2012, the *DF-PI-AERO* and *DF-PI-ENS* reconstructions show remarkable positive ΔGPP in low latitudes, while the ΔGPP of the other two reconstructions remain negative in most latitudes. The seasonal variations of ΔGPP from the different reconstructions are generally small compared to the latitude variability of ΔGPP derived from each experiment.

8
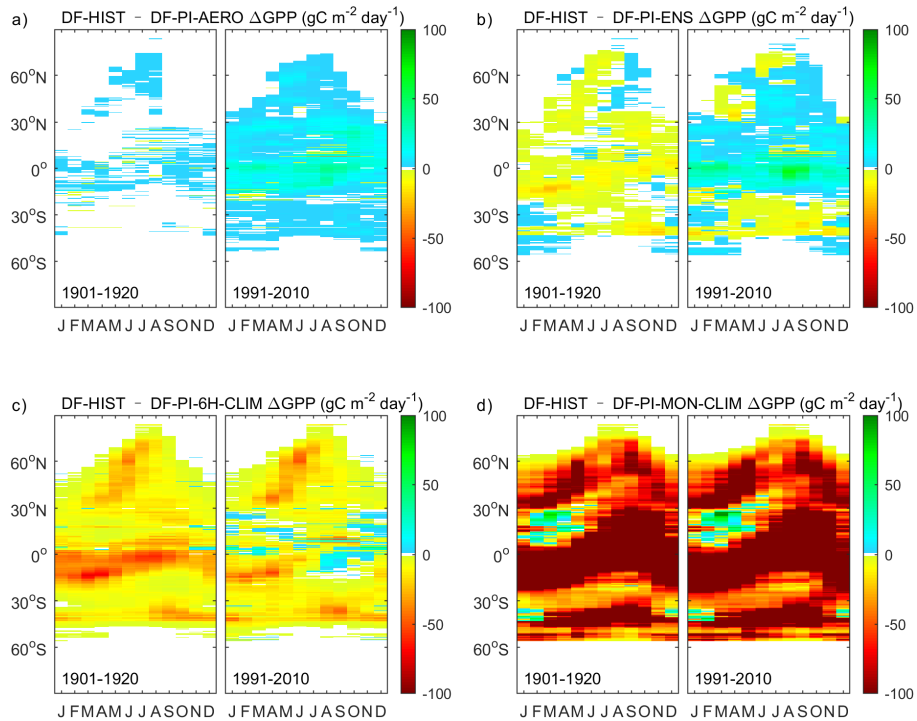
Figure 4. Seasonal variations of ΔGPP in gC m^{-2} day^{-1} between *DF-HIST* and (a) *DF-PI-AERO* , (b) *DF-PI-ENS* , (c) *DF-PI-6H-CLIM* and (d) *DF-PI-MON-CLIM* during 1901-1920 and 1991-2010.

In terms of the diurnal cycle of ΔGPP , different reconstructions show very different patterns (Fig. 5). The ΔGPP from the
DF-PI-AERO reconstruction shows remarkable positive values in the low latitudes during 2001-2005, with the largest ΔGPP in the late morning. Similarly, the *DF-PI-ENS* simulations also show positive ΔGPP in late morning in low latitudes during the same period. However, in midlatitudes of the Southern Hemisphere, the *DF-PI-ENS* ΔGPP is negative. In contrast to *DF-PI-AERO* and *DF-PI-ENS* , the *DF-PI-6H-CLIM* reconstruction has negative ΔGPP in most latitudes and the largest ΔGPP mainly occurs in the morning. Because the *DF-PI-MON-CLIM* reconstruction smoothed out the diurnal cycle of Fdf, its ΔGPP diurnal cycles show very different pattern compared with other reconstructions. In almost all latitudes, the *DF-PI-MON-CLIM* ΔGPP show large negative values in the afternoon. While in the morning, positive ΔGPP is found in latitudes 10°N-30°N and around 30°S.

4   Discussion

4.1   How does Fdf affect GPP?

The changes of diffuse radiation in natural conditions are often caused by changes in aerosols or cloud cover. Although many previous studies have reported larger light use efficiency under cloudier conditions or conditions with more aerosols, it is only
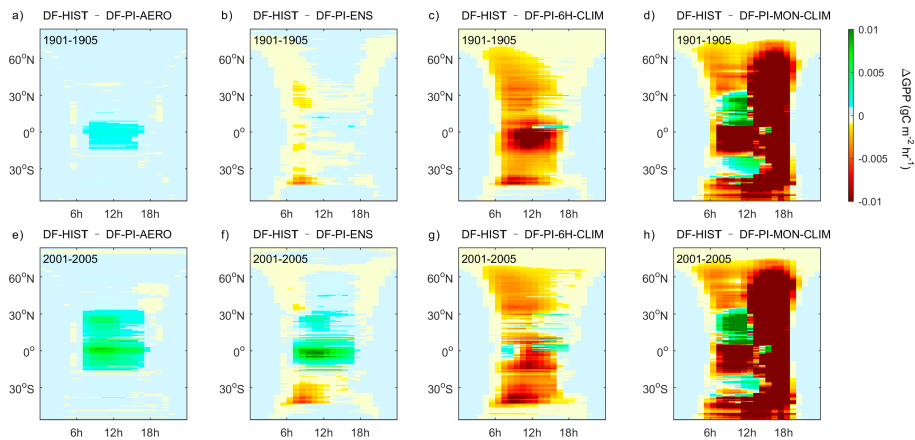
Figure 5. Diurnal variations of ΔGPP in gC m^{-2} hr^{-1} between *DF-HIST* and *DF-PI-AERO* (a,e), *DF-PI-ENS* (b,f), *DF-PI-6H-CLIM* (c,g) and *DF-PI-MON-CLIM* (d,h) during 1901-1905 (a-d) and 2001-2005 (e-h).

recently that it has been fully appreciated that this enhancement in light use efficiency is due to both changes in Fdf and other climate factors such as air temperature and VPD (Cheng *et al.* , 2015; Wang *et al.* , 2018; Zhang *et al.* , 2020) that covary with Fdf. In this study, we investigated the impact of Fdf alone for which there are several explanations (e.g., (Roderick *et al.* , 2001; Kivalov and Fitzjarrald, 2019)). Among these, the most widely accepted explanation is that compared with direct radiation which can be more easily blocked by leaves in the upper part of the canopy, diffuse radiation has more chance to get absorbed by shaded leaves (Li *et al.* , 2014), especially in thick canopies with a large leaf area index. Therefore, a larger Fdf will lead to more homogeneous distribution of light in canopy. Because the light-photosynthesis response curve at leaf level is a concave function (i.e., the mean photosynthesis rate of two light levels is smaller than the photosynthesis rate at the light level equal to the average of the two). Due to this mechanism, the impacts of Fdf on GPP should be larger when there are more shaded leaves in canopy (larger LAI) and when more sunlit leaves are light-saturated (stronger incoming shortwave radiation). This generally explains the spatial pattern of ΔGPP detected in this study (Fig. 3a).

4.2 Why using a climatological average of the diffuse light fraction to force a LSM results in a negative bias of pre-industrial GPP?

The impacts of Fdf on GPP depend on the level of radiation, therefore, it is necessary to get consistent Fdf and radiation forcing on 6-hourly to multi-annual time scales to correctly simulate GPP and consequently the Fdf impacts. However, there is no statistical method to keep the consistency of Fdf and radiation in a counterfactual no-anthropogenic-aerosol scenario. Compared with the *DF-HIST* scenario, the *DF-PI-MON-CLIM* Fdf reconstruction averaged out the diurnal cycle of Fdf. Because the solar zenith angle is large due to longer light path in atmosphere in the morning and afternoon, the Fdf is usually large in the morning and afternoon but low at midday (Iziomon and Aro , 1998). Prescribing the same monthly average of Fdf each 6-hourly time step in the *DF-PI-MON-CLIM* reconstruction thus underestimates the Fdf in the morning and afternoon when the radiation is

low and atmosphere scattering makes light predominantly diffuse, and overestimates the midday Fdf when the radiation is high. Thus, the use of the *DF-PI-MON-CLIM* method can cause a higher GPP during daytime but has a marginal impact on GPP in early morning and late afternoon. At global scale, this overestimation of GPP lead to a -12 PgC yr^{-1} ΔGPP (Fig. 2), much smaller than all the other reconstructions. It should be noted that the original 6-hourly Fdf data does not cover all timesteps. The model filled the absent value of Fdf with a unity (1) value (i.e. all radiation is diffuse) when the sun is below the horizon and interpolated this value to 30-min time steps for GPP calculation. In the *DF-PI-MON-CLIM* Fdf reconstruction, all time steps are filled with an average value. If the absent values happen to be before dawn, the data-filling procedure may result in spurious positive ΔGPP (Fig. 5d,h). This artifact is expected to get corrected when the Fdf field is provided at higher temporal resolution or if better interpolation techniques are used. Nevertheless, this regional positive ΔGPP does not alter the global negative ΔGPP detected by the *DF-PI-MON-CLIM* reconstruction (Fig. 2).

Compared with *DF-PI-MON-CLIM* , the *DF-PI-6H-CLIM* reconstruction did not smooth the diurnal cycle of Fdf. However, the GPP under *DF-PI-6H-CLIM* reconstruction is still overestimated (Fig. 2). This overestimation is also from the smooth of Fdf, not the diurnal cycle but the interannual variability of Fdf. Because the Fdf is affected by the scattering of aerosols and clouds, for a given solar zenith angle, the Fdf should be negatively correlated to the total radiation reaching the canopy (Spitters, 1986; Weiss and Norman, 1985). Due to this negative relationship between radiation and Fdf, the average of Fdf at the same time over years (solar position constant) actually underestimates the Fdf under most low radiation conditions but overestimates the Fdf under most high radiation conditions. As shown in Fig. 1, there are much few cases of extremely sunny (Fdf<0.3) or extremely cloudy (Fdf>0.9) conditions in the *DF-PI-6H-CLIM* reconstruction (Fig. 1b) than in the original Fdf field (Fig. 1a). As a result, the smoothing of the Fdf interannual variability in the *DF-PI-6H-CLIM* reconstruction causes an overestimation of the total GPP in a similar way as for the *DF-PI-MON-CLIM* reconstruction.

In contrast to the *DF-PI-6H-CLIM* and *DF-PI-MON-CLIM* reconstructions, the *DF-PI-ENS* simulations does not smooth Fdf. As a result, the Fdf mismatch with radiation is independent from the radiation level, although the Fdf remains inconsistent with the synoptic and inter-annual variability of shortwave light and other climate variables. The small range of the ΔGPP from the three ensemble members (Fig. 2) further indicates that the mismatch of Fdf among years does not essentially affect the GPP estimation.

Compared with the *DF-PI-6H-CLIM* , *DF-PI-MON-CLIM* and *DF-PI-ENS* reconstructions, the *DF-PI-AERO* used atmospheric radiative transfer model to partition the radiation into direct and diffuse components based on aerosol optical depth on a 6-hourly time step during the entire period. In this way, the Fdf variation remains consistent with the variations of radiation at all time scales. As expected, there is almost no bias in ΔGPP at the pre-industrial period (Fig. 2, 4 and 5).

Considering the ΔGPP bias could be also affected by the bias in total diffuse radiation due to the mismatch of Fdf and total radiation, we further investigate the global mean diffuse radiation over all time steps in each reconstruction. We find that different reconstructions have significant different mean diffuse radiation (Fig. 6). However, the difference in diffuse radiation bias and the bias in ΔGPP are not consistent (Fig. 2). For instance, the *DF-PI-6H-CLIM* and *DF-PI-ENS* reconstructions share similar mean diffuse radiation but differ significantly in ΔGPP. This difference implies that the mismatch between Fdf and radiation is more important than the mean diffuse radiation over a long period. Nevertheless, GPP always differs
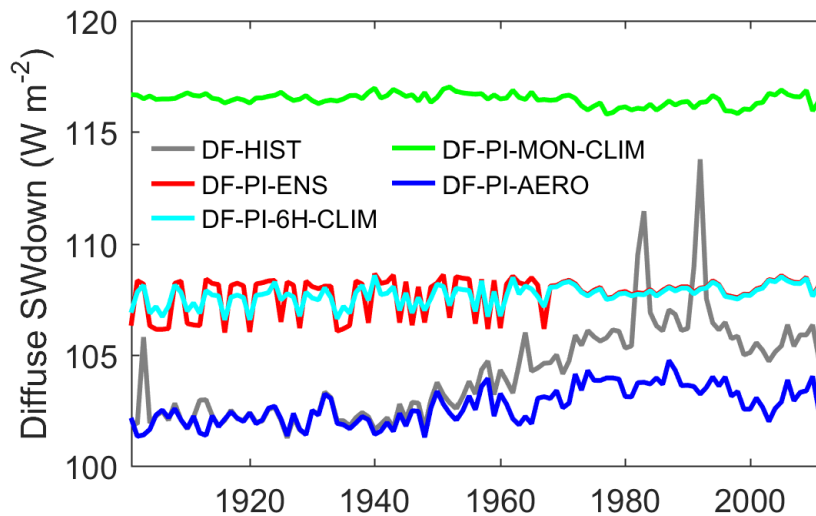
Figure 6. Mean diffuse incoming shortwave radiation at the surface from each reconstruction.

between LSMs. The magnitude of the GPP bias due to the mismatch between Fdf and SWdown detected here is only for ORCHIDEE_DF model and needs to be further investigated in other LSMs. Nevertheless, the framework that we propose is applicable to any LSM

265 ### 4.3 Recommendations for defining a baseline pre-industrial climate forcing inclusive of diffuse light

As discussed above, different diffuse radiation reconstruction techniques can result in strongly different ΔGPP in simulations. Therefore, it is important to have a reliable technique for scenario reconstruction and for diffuse radiation investigation.

By comparing the reconstructions used in this study, we argue that the *DF-PI-AERO* reconstruction, i.e. using atmospheric radiative transfer model to calculate the Fdf using aerosol and cloud information, can best simulate the GPP under no-aerosol
270 scenario because the Fdf obtained from this method does not mismatch Fdf and solar radiation. Similar methods have been used in Rap *et al.* (2018) and Yue and Unger (2018). However, to reconstruct the Fdf field in this way needs detailed aerosol and cloud information, which is not always available. In absence of such data, statistical methods are the alternative choice to do the reconstruction. In this case, our simulations have shown that the decrease of variability in Fdf due to any averaging processes can cause systematic mismatch between Fdf and incoming solar radiation, which then biases the GPP. In contrast
275 to the averaging methods, the mismatch in the *DF-PI-ENS* reconstruction is more random and the bias in *DF-PI-ENS* GPP is relatively small with small inter-simulation differences. Here we recommend that in future investigations of the impact of diffuse radiation in LSM offline simulations, the no-aerosol scenario Fdf should be calculated from aerosol and cloud information directly. When the information is not available, in ensemble simulations, repeating or randomly repeating the full Fdf time series from one or several pre-industrial years could become an acceptable alternative.

Despite that both reconstructions are acceptable in detecting diffuse radiation impacts, the impacts detected by the *DF-PI-AERO* and *DF-PI-ENS* reconstructions are not exactly the same. This is because that the *DF-PI-ENS* reconstruction implicitly eliminated Fdf changes caused by all factors including aerosols and clouds, while the *DF-PI-AERO* here has varying cloud information. In this study, the impacts of cloud difference on GPP are much smaller than the bias caused by the problematic Fdf reconstructions (Fig. 2). However, we still cannot conclude with negligible cloud impacts because current cloud data remains very inaccurate.

5 Conclusions

For summary, in this study, we used different methods to reconstruct Fdf under no-anthropogenic-aerosol scenario and evaluated the influence of reconstruction methods on the diffuse radiation impacts on GPP using the ORCHIDEE_DF land surface model. We conclude that the traditional statistical methods by using a climatological average Fdf can cause 1-13 PgC yr^{-1} bias on global GPP. To correctly simulate GPP, Fdf reconstructions need to retain its full variability. Based on our results, we recommend to use pre-industrial aerosol information to calculate Fdf directly, or as an alternative in the absence of aerosol data, to use ensemble simulations driven by the original Fdf time series from pre-industrial years.

Besides the experimental designs investigated in this study, it is also possible to use coupled simulations in ESMs to investigate the impacts of aerosols. In this way, the experiments can be better controlled and the climate-carbon feedback caused by the aerosol impacts can be investigated. However, due to the larger complexity of earth system models compared to LSMs, the ESM experiments may suffer from larger uncertainties, which remain to get investigated.

6 Code and data availability

The code of the ORCHIDEE_DF used in this study is available at https://forge.ipsl.jussieu.fr/orchidee/wiki/GroupActivities/CodeAvalaibilityPublication/ORCHIDEE_DFv1.0_DFforc (Zhang , 2021). The CRUJRA data (Harris, 2019) and corresponding diffuse radiation fraction data used in this study is available at TRENDY ftp, details at http://sites.exeter.ac.uk/trendy/protocol

310   References

Alton, P., North, P., and Los, S.: The impact of diffuse sunlight on canopy light-use efficiency, gross photosynthetic product and net ecosystem exchange in three forest biomes, Global Change Biol., 13(4), 776–787, 2007a

Alton, P., Ellis, R., Los, S., and North, P.: Improved global simulations of gross primary product based on a separate and explicit treatment of diffuse and direct sunlight, J. Geophys. Res.-Atmos., 112, D07203, doi:10.1029/2006JD008022.1, 2007b

315   Bellouin, N., Rae, J., Jones, A., Johnson, C., Haywood, J., and Boucher, O.: Aerosol forcing in the Climate Model Intercomparison Project (CMIP5) simulations by HadGEM2-ES and the role of ammonium nitrate, J. Geophys. Res.-Atmos., 116, D20206, doi:10.1029/2011JD016074.1., 2011

Chen, Min. Evaluation of atmospheric aerosol and tropospheric ozone effects on global terrestrial ecosystem carbon dynamics, Ph.D. thesis, Purdue University, USA, 2013.

320   Cheng, S. J., Bohrer, G., Steiner, A. L., Hollinger, D. Y., Suyker, A., Phillips, R. P., and Nadelhoffer, K. J.: Variations in the influence of diffuse light on gross primary productivity in temperate ecosystems, Agr. Forest Meteorol., 201, 98-110, 2015

Choudhury, B. J.: Estimating gross photosynthesis using satellite and ancillary data: Approach and preliminary results, Remote Sens. Environ., 75(1), 1–21, 2001

Dai, Y., Dickinson, R. E., and Wang, Y.-P.: A two-big-leaf model for canopy temperature, photosynthesis, and stomatal conductance, J.
325   Climate, 17(12), 2281–2299, 2004

Eyring, V., Bony, S., Meehl, G. A., Senior, C. A., Stevens, B., Stouffer, R. J., and Taylor, K. E.: Overview of the Coupled Model Intercomparison Project Phase 6 (CMIP6) experimental design and organization, Geosci. Model Dev., 9, 1937-1958, 10.5194/gmd-9-1937-2016, 2016

Gu, L., Baldocchi, D., Verma, S. B., Black, T., Vesala, T., Falge, E. M., and Dowty, P. R.: Advantages of diffuse radiation for terrestrial
330   ecosystem productivity, J. Geophys. Res.-Atmos., 107(D6), ACL 2-1-ACL 2–23, 2002

Gu, L., Baldocchi, D. D., Wofsy, S. C., Munger, J. W., Michalsky, J. J., Urbanski, S. P., and Boden, T. A.: Response of a deciduous forest to the Mount Pinatubo eruption: Enhanced photosynthesis, Science, 299(5615), 2035–2038, 2003

Harris, I., Jones, P. D., Osborn, T. J., and Lister, D. H.: Updated high-resolution grids of monthly climatic observations–the CRU TS3. 10 Dataset, Int. J. Climatol., 34(3), 623–642., 2014

335   Harris, I.: CRU JRA v1.1: A forcings dataset of gridded land surface blend of Climatic Research Unit (CRU) and Japanese reanalysis (JRA) data; Jan. 1901 - Dec. 2017. Centre for Environmental Data Analysis, 25 February 2019. doi:10.5285/13f3635174794bb98cf8ac4b0ee8f4ed., 2019

Inness, A., Ades, M., Agusti-Panareda, A., Barré, J., Benedictow, A., Blechschmidt, A.-M., Dominguez, J., Jose, Engelen, R., Eskes, H., Flemming, J., Huijnen, V., Jones, L., Kipling, Z., Massart, S., Parrington, M., Peuch, V.-H., Razinger, M., Rémy, S., P, Schulz, M., and
340   Suttie, M.: The CAMS reanalysis of atmospheric composition, Atmos. Chem. Phys., 19, 3515-3556, 10.5194/acp-19-3515-2019, 2019.

Iziomon, M. G., and Aro, T. O.: The diffuse fraction of global solar irradiance at a tropical location, Theor. Appl. Climatol., 61, 77–84, 10.1007/s007040050053, 1998.

Kivalov, S. N., and Fitzjarrald, D. R.: Observing the whole-canopy short-term dynamic response to natural step changes in incident light: Characteristics of tropical and temperate forests, Bound.-Layer Meteorol., 173, 1–52, 10.1007/s10546-019-00460-5, 2019.

345   Kobayashi, S., Ota, Y., Harada, Y., Ebita, A., Moriya, M., Onoda, H., Onogi, K., Kamahori, H., Kobayashi, C., Endo, H., Miyaoka, K., and Takahashi, K.: The JRA-55 reanalysis: General specifications and basic characteristics, J. Meteorol. Soc. Jpn. Ser. II, 93, 5–48, 10.2151/jmsj.2015-001, 2015.

Krinner, G., Viovy, N., de Noblet-Ducoudré, N., Ogée, J., Polcher, J., Friedlingstein, P., Ciais, P., Sitch, S., and Prentice, I. C.: A dynamic global vegetation model for studies of the coupled atmosphere-biosphere system, Global Biogeochem. Cycles, 19, 2005.

350   Lamarque, J. F., Bond, T. C., Eyring, V., Granier, C., Heil, A., Klimont, Z., Lee, D., Liousse, C., Mieville, A., Owen, B., Schultz, M. G., Shindell, D., Smith, S. J., Stehfest, E., Van Aardenne, J., Cooper, O. R., Kainuma, M., Mahowald, N., McConnell, J. R., Naik, V., Riahi, K., and van Vuuren, D. P.: Historical (1850–2000) gridded anthropogenic and biomass burning emissions of reactive gases and aerosols: methodology and application, Atmos. Chem. Phys., 10, 7017-7039, 10.5194/acp-10-7017-2010, 2010.

Li, T., Heuvelink, E., Dueck, T., Janse, J., Gort, G., and Marcelis, L.: Enhancement of crop photosynthesis by diffuse light: Quantifying the
355   contributing factors, Ann. Bot.-London, 114(1), 145–156, 2014

Mercado, L. M., Bellouin, N., Sitch, S., Boucher, O., Huntingford, C., Wild, M., and Cox, P. M.: Impact of changes in diffuse radiation on the global land carbon sink, Nature, 458(7241), 1014–1017, 2009

Nemani, R. R., Keeling, C. D., Hashimoto, H., Jolly, W. M., Piper, S. C., Tucker, C. J., Myneni, R. B., and Running, S. W.: Climate-driven increases in global terrestrial net primary production from 1982 to 1999, Science, 300, 1560-1563, 10.1126/science.1082750, 2003.

360   Niyogi, D., Chang, H.-I., Saxena, V. K., Holt, T., Alapaty, K., Booker, F., Chen, F., Davis, K. J., Holben, B., Matsui, T., Meyers, T., Oechel, W. C., Pielke Sr., R. A., Wells, R., Wilson, K., and Xue, Y.: Direct observations of the effects of aerosol loading on net ecosystem CO_2 exchanges over different landscapes, Geophys. Res. Lett., 31, 10.1029/2004gl020915, 2004.

Rap, A., Scott, C. E., Reddington, C. L., Mercado, L., Ellis, R. J., Garraway, S., Evans, M. J., Beerling, D. J., MacKenzie, A. R., Hewitt, C. N., and Spracklen, D. V.: Enhanced global primary production by biogenic aerosol via diffuse radiation fertilization, Nat. Geosci., 11,
365   640–644, https://doi.org/10.1038/s41561-018-0208-3, 2018.

Roderick, M. L., Farquhar, G. D., Berry, S. L., and Noble, I. R.: On the direct effect of clouds and atmospheric particles on the productivity and structure of vegetation, Oecologia, 129(1), 21–30, 2001

Sato, M., Hansen, J. E., McCormick, M. P., and Pollack, J. B.: Stratospheric aerosol optical depths, 1850–1990, J. Geophys. Res.-Atmos., 98, 22987–22994, 10.1029/93jd02553, 1993.

370   Spitters, C., Toussaint, H., and Goudriaan, J.: Separating the diffuse and direct component of global radiation and its implications for modeling canopy photosynthesis Part I. Components of incoming radiation, Agr. Forest Meteorol., 38, 217-229, 1986.

Thomason, L. W., Ernest, N., Millán, L., Rieger, L., Bourassa, A., Vernier, J.-P., Manney, G., Luo, B., Arfeuille, F., and Peter, T.: A global space-based stratospheric aerosol climatology: 1979–2016, Earth Syst. Sci. Data, 10, 469–492, https://doi.org/10.5194/essd-10-469-2018, 2018.

375   Wang, X., Wu, J., Chen, M., Xu, X., Wang, Z., Wang, B., Wang, C., Piao, S., Lin, W., Miao, G., Deng, M., Qiao, C., Wang, J., Xu, S., and Liu, L.: Field evidences for the positive effects of aerosols on tree growth, Global Change Biol., 24, 4983-4992, 10.1111/gcb.14339, 2018.

Weiss, A., and Norman, J.: Partitioning solar radiation into direct and diffuse, visible and near-infrared components, Agr. Forest Meteorol., 34(2-3), 205–213, 1985

Yue, X. and Unger, N.: Aerosol optical depth thresholds as a tool to assess diffuse radiation fertilization of the land carbon uptake in China,
380   Atmos. Chem. Phys., 17, 1329–1342, https://doi.org/10.5194/acp-17-1329-2017, 2017.

Yue, X., and Unger, N.: Fire air pollution reduces global terrestrial productivity, Nat. Commun., 9, 5413. https://doi.org/10.1038/s41467-018-07921-4, 2018

Zhang, Y., Goll, D., Bastos, A., Balkanski, Y., Boucher, O., Cescatti, A., Collier, M., Gasser, T., Ghattas, J., Li, L., Piao, S., Viovy, N., Zhu, D., and Ciais, P.: Increased global land carbon sink due to aerosol-induced cooling, Global Biogeochem. Cycles, 33, 439–457,

385   10.1029/2018gb006051, 2019.

Zhang, Y.: ORCHIDEE_DFv1.0_DFforc, https://forge.ipsl.jussieu.fr/orchidee/wiki/GroupActivities/CodeAvalaibilityPublication/ORCHIDEE_DFv1.0_D 2021.

Zhang, Y., Bastos, A., Maignan, F., Goll, D., Boucher, O., Li, L., Cescatti, A., Vuichard, N., Chen, X., Ammann, C., Arain, M. A., Black, T. A., Chojnicki, B., Kato, T., Mammarella, I., Montagnani, L., Roupsard, O., Sanz, M. J., Siebicke, L., Urbaniak, M., Vaccari, F. P.,

390   Wohlfahrt, G., Woodgate, W., and Ciais, P.: Modeling the impacts of diffuse light fraction on photosynthesis in ORCHIDEE (v5453) land surface model, Geosci. Model Dev., 13, 5401–5423, https://doi.org/10.5194/gmd-13-5401-2020, 2020.